Author(s): Lázaro, Ariadna; Cunha, Carla; Bosque, Ramon; Pina, João; Ward, Jas S.; Truong, Khai-Nghi; Rissanen, Kari; Lima, João Carlos; Crespo, Margarita; Seixas de Melo, J. Sérgio; Rodríguez, Laura

Title: Room-Temperature Phosphorescence and Efficient Singlet Oxygen Production by Cyclometalated Pt(II) Complexes with Aromatic Alkynyl Ligands

Year: 2020

Version: Accepted version (Final draft)

Please cite the original version:

Lázaro, A., Cunha, C., Bosque, R., Pina, J., Ward, J. S., Truong, K.-N., Rissanen, K., Lima, J. C., Crespo, M., Seixas de Melo, J. S., & Rodríguez, L. (2020). Room-Temperature Phosphorescence and Efficient Singlet Oxygen Production by Cyclometalated Pt(II) Complexes with Aromatic Alkynyl Ligands. Inorganic Chemistry, 59(12), 8220-8230. https://doi.org/10.1021/acs.inorgchem.0c00577

Room Temperature Phosphorescence and efficient singlet oxygen production by cyclometallated Pt(II) complexes with aromatic alkynyl ligands

Ariadna Lázaro,[a,b] Carla Cunha,[c] Ramon Bosque,[a] João Pina,[c] Jas S. Ward,[d] Khai-Nghi Truong,[d] Kari Rissanen,[d] João Carlos Lima,[e] Margarita Crespo,[a,f] J. Sérgio Seixas de Melo[c,*] and Laura Rodríguez[a,b,*]

[a] *Departament de Química Inorgànica i Orgànica, Secció de Química Inorgànica, Universitat de Barcelona, Martí i Franquès 1-11, E-08028 Barcelona, Spain. e-mail: laura.rodriguez@qi.ub.es*

[b] *Institut de Nanociència i Nanotecnologia (IN2UB). Universitat de Barcelona, 08028 Barcelona, Spain*

[c] *Coimbra Chemistry Centre, Department of Chemistry, University of Coimbra, Rua Larga, Coimbra 3004-535, Portugal. e-mail: sseixas@ci.uc.pt*

[d] *Department of Chemistry, P.O. Box 35, 40014, Jyväskylä, Finland*

[e] *LAQV-REQUIMTE, Departamento de Química, Universidade Nova de Lisboa, 2829-516 Monte de Caparica, Portugal*

[f] *Institut de Biomedicina de la Universitat de Barcelona (IBUB), 08028-Barcelona, Spain*

Abstract

The synthesis of five novel cyclometallated platinum(II) compounds containing five different alkynyl-chromophores was achieved by the reaction of the previously synthesized Pt-Cl cyclometallated compound (**1**) with the corresponding RC≡CH by a Sonogashira reaction. It was observed that the spectral and photophysical characteristics of the cyclometallated platinum(II) complexes (Pt-Ar) are essentially associated to the platinum-cyclometallated unit. Room temperature emission of the Pt-Ar complexes was attributed to phosphorescence in agreement with DFT calculations. Broad nanosecond (ns)-transient absorption spectra were observed with decays approximately identical to those obtained from the emission of the triplet state. From the femtosecond-transient absorption (fs-TA) data two main excited state decay components were identified: one in the order of few ps assigned to fast intersystem crossing to populate the triplet excited-state and the second (hundreds of ns) associated to the decay of the transient triplet state. In general, efficient singlet oxygen photosensitization quantum yields were observed from the triplet state of these complexes.

Keywords: Platinum, luminescence, photophysics, cyclometallated, singlet state, triplet state, RTP (room temperature phosphorescence)

Introduction

Organometallic π-conjugated materials have emerged as a frontier research field over the past few decades, owing to their application in organic light emitting diodes, organic photovoltaic devices, and as materials for nonlinear absorption.[1] In particular, cyclometallated complexes of late transition metals attract vast interests, mainly for their outstanding luminescent properties. Such complexes typically feature pronounced ligand-involved components (e.g., MLCT or ILCT) in their lowest triplet excited state, which facilitate radiative decays, turning emission into a competitive pathway in relation to the non-radiative relaxation processes. The photophysical properties of the cyclometallated complexes are therefore sensitively influenced by both the cyclometallated and ancillary ligands, making possible for more convenient tailoring of the photophysical properties by changing and modifying the ligand structures.[2] On the other hand, heavy atom-containing π-conjugated complexes are unique in achieving efficient nonlinear absorption by a "dual mode" pathway because of the facility of harvesting triplet excited states via the spin−orbit coupling effect.[3,4] In particular, the presence of heavy-metal ion enhances the intersystem crossing (ISC) process which is usually competitive with fluorescence. As a result, many of these complexes show dual fluorescence and phosphorescence emission.

In general, singlet excited states (^{1}MLCT and ^{1}LC) first formed by cyclometallated complexes upon photo-excitation quickly undergo ISC to the triplet excited states with high efficiency. The lowest triplet excited state is typically described as a mixed ^{3}MLCT/^{3}LC state,[2] but can include also ^{3}ILCT, ^{3}LLCT, ^{3}LMMCT, ^{3}MMLCT, or ^{3}MLLCT states.[1] Consequently, these complexes have gained great interest in numerous applications including dopants in OLEDs, photocatalysts, biological labelling reagents, optical sensors, nonlinear optical materials, solid-state light-emitting electrochemical cells or photodynamic therapy (PDT) photosensitizers.[5–12] One of the most intensively investigated classes of PDT photosensitizers are the cyclic tetrapyrrolic derivatives, such as porphyrins (including texaphyrins), phthalocyanines and chlorins, but these systems suffer from certain drawbacks, such as the difficulty for modulating their photophysical and biological properties through chemical modifications.[13] For this reason, there is a growing interest for developing new compounds, such as cyclometallated complexes for which the photophysical parameters can be systematically tuned by changes of the electronic properties of the complex as for porphyrins and phthalocyanines.[13] One of the first reports on cyclometallated Pt(II) complexes used for singlet oxygen sensitization was

contributed by Weinstein and co-workers in 2006[14] and some other Pt(II) cyclometallated complexes with more or less efficiency have been published up to date.[2] The higher efficiency of Pt(II) over other heavy atoms such as Ir(III) is attributed to its square-planar geometry that avoids steric hindrances and eases the interaction with dioxygen molecule.

Taking all of this into consideration, in this work, we have designed and synthesized a series of five new Pt(II) cyclometallated compounds that differ on the ancillary ligand which is an alkynyl-chromophore. Some examples of luminescent Pt [C^N^N] cyclometallated complexes have already been reported in the literature and, to the best of our knowledge, in all of them the three [C^N^N] coordination positions belong to an aromatic cycle.[15–19] The photophysical characterization of Pt [C^N^N] cyclometallated compounds containing a tridentate [C^N^N'] imine ligand and alkynylchromophoric units occupying the forth coordination position of the metal sphere is herein reported for the first time. Their potential as photosensitizers for singlet oxygen production was also evaluated.

Results and Discussion

Synthesis and Characterization

The syntheses of the compounds were carried out following the strategy summarized in Scheme 1 by slight modifications of the previously reported Sonogashira method.[20] The parent cyclometallated compound **1** reacted with the alkynyl aromatic chromophore RC≡CH in the presence of sodium acetate as a base and CuI as a catalyst.

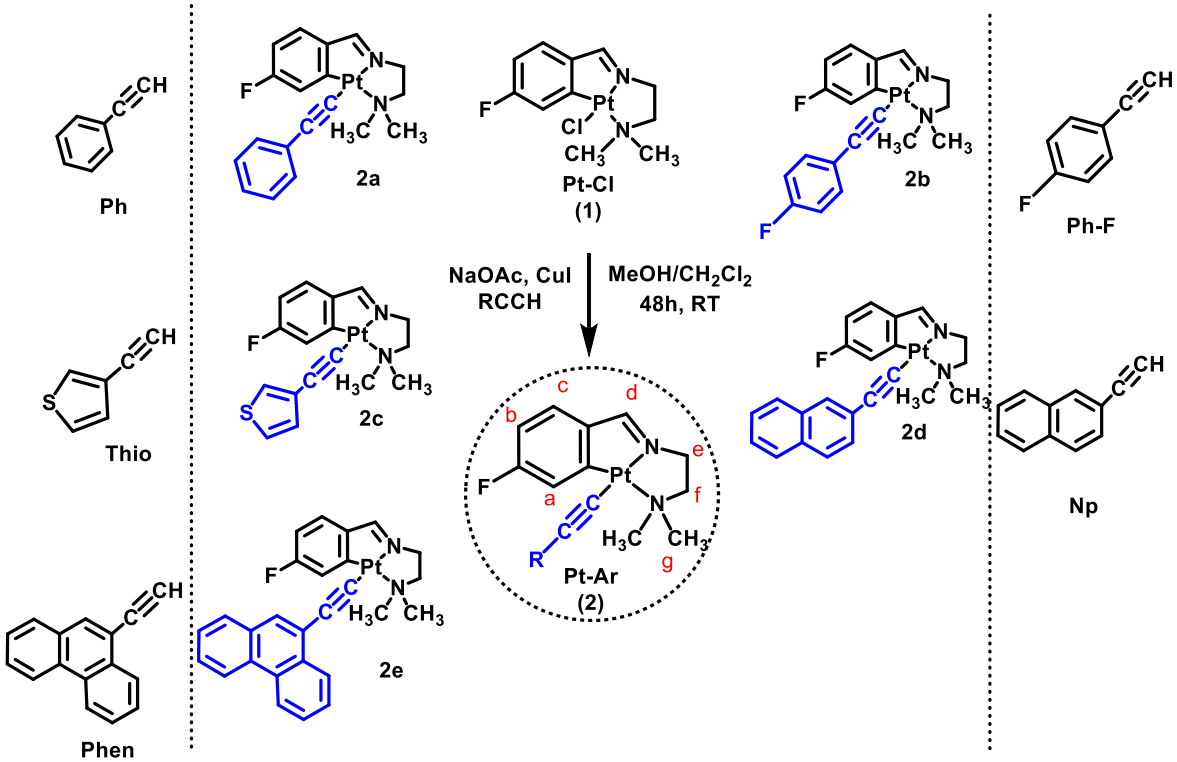

Scheme 1. Synthesis, structures and acronyms of the cyclometallated Platinum(II) complexes (named Pt-Ar, at the centre of the picture) and of the uncoordinated ligands (left and right hands of the picture). The letters in Pt-Ar (2) are used for NMR assignment.

The compounds were obtained as orange solids after precipitation and washing with hexane in moderate-high yields (55-85%).

All compounds were characterized by mass spectra and ^{1}H and ^{19}F NMR spectra. ^{1}H NMR of all compounds display the disappearance of the terminal alkynyl proton as a direct indication of coordination together with the corresponding protons of this new ancillary ligand. As previously observed, the dimethylamino protons H^{g} appear as a singlet around 3 ppm integrating for 6 H and coupled to platinum and the imine proton is

also coupled to platinum. Additionally, H^a aromatic proton is also observed to couple to platinum with a ^3J(Pt-H) of *ca*. 70.2 Hz. The ^{19}F NMR spectra show only one signal, as a broad singlet, which is not significantly affected by the exchange of chloride to alkynyl-aromatic group. A second signal is present in the NMR of compound **2b** due to the aromatic *p*-fluorobenzene moiety (Figures S1-S10 in SI).

Further confirmation of the successful formation of the product was gained from the C≡C vibration determined by IR spectroscopy and by the determination of the protonated molecular peak in all cases recorded by ESI(+) spectrometry (Figures S11-S15 in SI).

Single crystals suitable for X-ray diffraction analysis were grown for **2b**, **2c** and **2d** (Figure 1 and Table S1). One single molecule is present in the asymmetric unit of **2b** and **2d** while three independent molecules are observed in the asymmetric unit of **2c** (Figure S16). Pt···Pt distances are ca. 3.9 and 4.4 Å and thus, metallophilic interactions are excluded in this asymmetric unit. The unit cells, shown in Figures S17-S19 (A), contain four (**2b** and **2d**) or twelve molecules (**2c**). As expected, in all cases the platinum adopts a square-planar coordination completed with the tridentate [C^N^N'] ligand and an alkynyl-chromophorê ligand *trans* to the imine. Bond lengths and angles are in the same range than those previously reported in the literature for Pt(II) cyclometallated complexes.[11,12] The alkynyl chromophore is at near linear conformation with the Pt metal atom, with angles around 170º-175º and its aromatic ring is almost perpendicular to the square-planar [C^N^N']-Pt plane. The 3D packing of **2c** and **2d** shows intermolecular short contacts involving the fluorine atom (F(1)···H(9b) = 2.551 Å for **2c** and F(1)···H(17) = 2.552 Å for **2d**), while for **2b** the most relevant intermolecular short contacts involve the platinum atom or the alkynyl moiety (Pt(1)···H(21) = 2.782 Å and C(15)···H(9B) = 2.689 Å), as depicted in Figures S17-S19 (B).

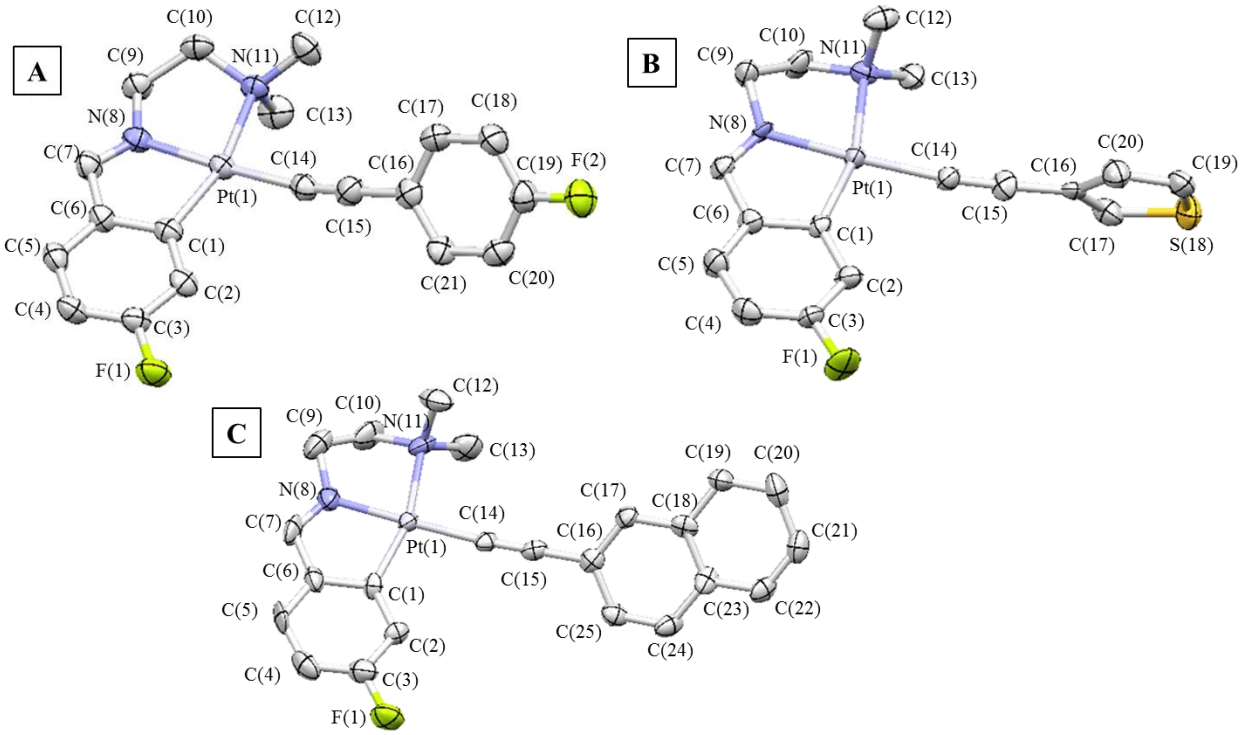

Figure 1. Molecular structures of compounds **2b** (A), **2c** (B) and **2d** (C). Selected bond lengths (Å) and angles (deg.) with estimated standard deviations. For **2b**: Pt(1)–N(8): 2.010(6); Pt(1)–N(11): 2.176(5); Pt(1)–C(14): 2.002(7); Pt(1)–C(1): 1.999(6); C(14)–C(15): 1.161(9); N(8)–Pt(1)–N(11): 81.9(2); C(1)–Pt(1)–N(8): 81.5(2); C(1)–Pt(1)–C(14): 97.2(3); C(14)–Pt(1)–N(11): 99.1(2); Pt(1)-C(14)-C(15): 170.05; for **2c**: Pt(1)–N(8): 2.001(11); Pt(1)–N(11): 2.157(12); Pt(1)–C(14): 1.992(15); Pt(1)–C(1): 1.984(14); C(14)–C(15): 1.180(2); N(8)–Pt(1)–-N(11): 81.6(5); C(1)–Pt(1)–N(8): 81.6(5); C(1)–Pt(1)–C(14): 100.0(6); C(14)–Pt(1)–N(11): 96.7(5); Pt(1)-C(14)-C(15): 174.03; for **2d**: Pt(1)–N(8): 1.990(11); Pt(1)–N(11): 2.161(11); Pt(1)–C(12): 1.963(13); Pt(1)–C(7): 2.005(14); C(12)–C(13): 1.199(18); N(8)–Pt(1)–N(11): 82.4(5); C(7)–Pt(1)–N(8): 81.5(5); C(7)–Pt(1)–C(12): 98.1(5); C(12)–Pt(1)–N(11): 98.1(5); Pt(1)-C(14)-C(15): 174.72. The thermal ellipsoids are drawn at the 50% probability level.

Electronic Spectral and Photophysical Characterization

The absorption spectra of the platinum(II) compounds **1** (Pt-Cl) and **2a-e** (Pt-Ar) show several bands in the UV-Visible range with moderate molar extinction coefficient, ε, values (Figure 2 and Table 1). The lowest energy band with maxima at around 380 nm can be attributed to Pt(5d) - π*(L) metal-to-ligand charge transfer (MLCT) mixed with intraligand transitions.[6,12,21–23] A higher energy absorption band is also observed in the 280-300 nm range with higher ε values which is also recorded for the uncoordinated alkynyl ligands, and for this reason, it can be assigned to π–π* intraligand transitions.[11]

Additional intraligand transitions typical for phenanthryl or naphthyl chromophores are buried under the absorption of the complexes. DFT theoretical calculations support these assignments (see below).

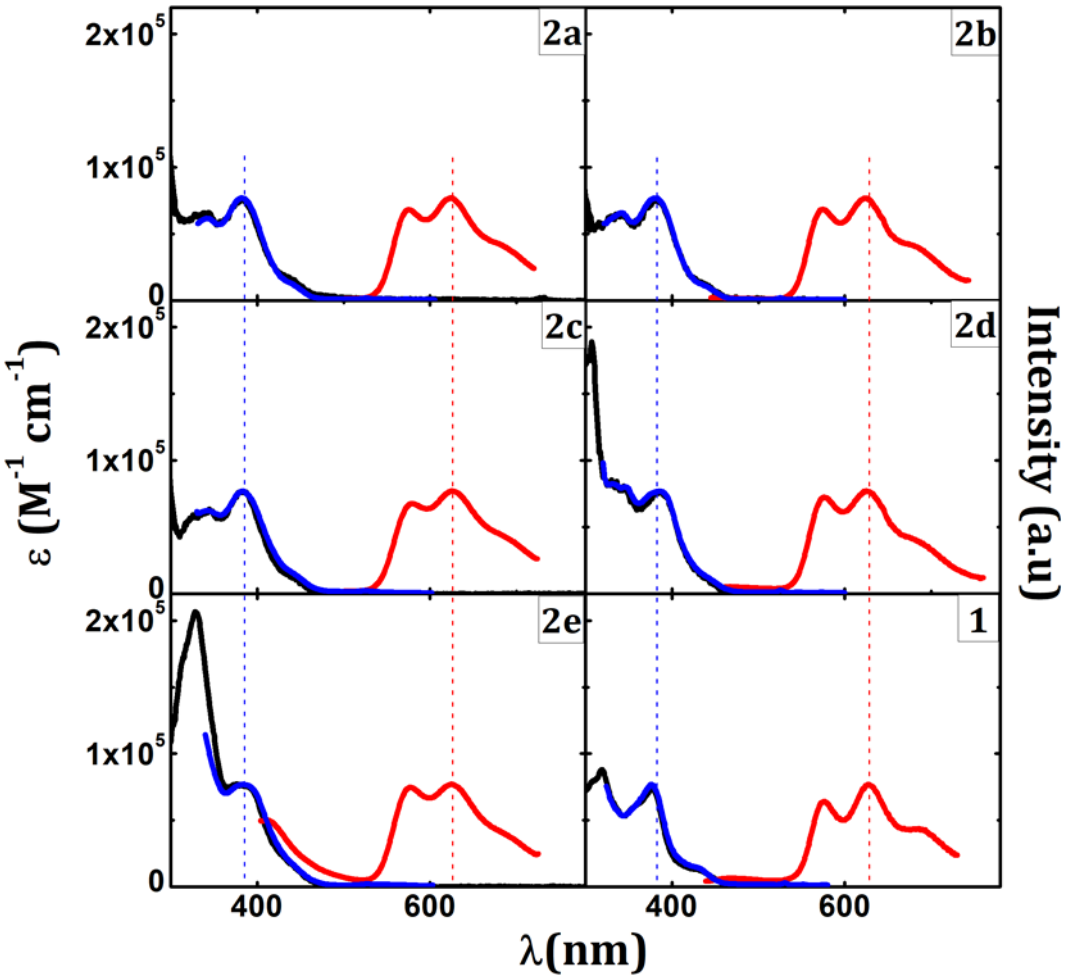

Figure 2. Normalized absorption (black line) together with the phosphorescence excitation (blue line) and emission (red line) spectra for 1.3×10^{-5} M acetonitrile solutions of the Pt-Ar complexes **(2a-e)** and Pt-Cl (**1**) at 293 K.

It is thus clear from the absorption spectra that the cyclometallated unit dominates the spectral features of these compounds (similar profiles were observed for **1** and **2a-e**, see Figure 2), which is in agreement with the fact that (via visual observation) the new alkynyl aromatic ligands do not affect the resulting color of the powders. Moreover, the absorption spectra of the Pt-Ar complexes (Figures 2 and S20) match the excitation (Figure S21) spectra, as a proof of the purity of the complexes thus showing that the emissive species are populated by both the Pt-cyclometallated and alkynyl-chromophore units.

The luminescence spectra of the Pt-Ar compounds show a vibronically structured band centered at *ca*. 625 nm, found independent of the excitation wavelength (Figure 2). The vibronic structure of the band with progressional spacing of 1200 cm^{-1}, typical of ν(C=C) and ν(C=N) stretching frequencies, demonstrates the involvement of the ligand character in their emission origin. The large Stokes' shift and the quenching of the band intensity in the presence of oxygen (Table 1 and Figure S22) strongly indicate the origin of this luminescence to be the emission from the triplet state, i.e., phosphorescence emission. This is further confirmed from ns- and fs-TA data and DFT calculations and is characteristic of platinum complexes due to heavy atom effect, which enhances the triplet state population and, consequently, the phosphorescence emission. Taking these facts into consideration, and the same profile observed in all cases, the observed emission can be attributed to ^{3}IL that can be mixed with ^{3}MLCT transitions, involving the cyclometallated ligand. The value of the obtained lifetimes for the Pt-Ar complexes, in the range 350-580 ns (Table 2), supports a triplet origin where the $T_1 \rightarrow S_0$ transition become significantly allowed by the presence of the enhanced spin orbit coupling induced by Pt metal atom.

Table 1. Spectral data (including wavelength absorption, molar extinction coefficients, ε (in brackets), phosphorescence emission maxima, and Stokes shift, Δ_{ss} (cm^{-1})) for the Pt-Ar complexes in acetonitrile (MeCN) at room temperature (293K) and transient $T_1 \rightarrow T_n$ maxima.

Compound	$\lambda_{abs,}$ **nm** **($\varepsilon \times 10^{-3}$, M^{-1} cm^{-1})**	λ_{em}^{max} **(nm)**	$\lambda_{max}^{T_1 \rightarrow T_n}$ **(nm)**	Δ_{ss} **(cm^{-1})**
1	**378** (7.7)	**629**	460	10557
2a	**282** (21.6), **342** (6.6), **382** (7.6)	**624**	540	10152
2b	**278** (21.2), **342** (6.9), **382** (7.7)	**625**	540	10178
2c	**280** (14.7), **342** (5.6), **382** (6.2)	**626**	540	10204
2d	**297** (8.0), **309** (8.2), **386** (7.1)	**626**	490	9932
2e	**333** (10.1), **380** (7.5)	**624**	540	10290

The phosphorescence quantum yields are lower than for other cyclometallated Pt [C^N^N] complexes reported in the literature and it may be ascribed to the more flexible imine ligand in comparison with the more rigid aromatic Pt [C^N^N] compounds.[15]

Table 2 - Room temperature photophysical parameters including phosphorescence quantum yields, f_{Ph}, and lifetimes, τ_{Ph}^{o}, (obtained using the Time Correlated Single Photon counting technique), together with triplet-state lifetimes (from ns-ms laser flash photolysis), singlet oxygen sensitization quantum yields (ϕ_{Δ}), internal conversion quantum yields (ϕ_{IC}) and associated rate constants, k_{ET}, radiative phosphorescence decay, k_{Ph}, and intersystem crossing, $k_{ISC}^{T_1 \sim \rightarrow S_0}$, obtained in aerated (with O_2) or degassed (N_2 sat.) acetonitrile solutions for the Pt-Ar and the parent compound **1**.

Compound	f_{Ph} **(with O_2)**	f_{Ph}^{0} **(N_2 sat.)**	τ_{Ph}^{o} **(ns) (N_2 sat.)**	τ_T **(ns) (N_2 sat.)**	f_D **(with O_2)**	$\Phi_{IC}^{S_1 \rightarrow S_0}$ a)	k_{ET} **x10^6 (s)**	k_{Ph} **x10^6(s)**	$k_{ISC}^{T_1 \sim \rightarrow S_0}$ **x10^6(s)**
1	0.005	0.016	353	423	0.47	0.53	6.23	0.07	2.76
2a	0.005	0.023	438	630	0.21	0.79	8.21	0.20	2.09
2b	0.007	0.023	491	700	0.11	0.89	4.66	0.30	1.74
2c	0.009	0.018	557	650	0.29	0.71	1.80	0.06	1.74
2d	0.008	0.025	464	700	0.12	0.88	4.58	0.31	1.85
2e	0.008	0.028	579	1200	0.16	0.84	4.32	0.22	1.51

a) $\Phi_{IC}^{S_1 \rightarrow S_0} = 1 - \phi_F - \phi_T$, assuming $\phi_F \sim 0$ and unitary singlet oxygen sensitization efficiency, $S_D = \frac{f_T}{f_D} = 1$ and therefore $\phi_T \cong f_D$.

ns-Transient Absorption

Time-resolved transient absorption spectra in the ns-TA and fs-TA were recorded in order to get further insights into the characteristics of the excited states formed. The transient triplet-triplet absorption spectra recorded by laser flash photolysis at 355 nm (ns-TA) of degassed acetonitrile solutions of the Pt-Ar derivatives, in addition to ground-state depletion (in the 380-410 nm range), present intense broad triplet-triplet absorption bands ranging between 420 nm and 700 nm, see Figure 3. Inspection of the spectra and the data summarized in Table 1 shows that the transient triplet-triplet wavelength maxima are

basically constant for the five platinum-alkynyl cyclometallated compounds **2a-e**, ranging from 490-540 nm, thus showing that the triplet state is much more localized and essentially corresponding to a chromophore unit which is the basic structure of the Pt-Cl (**1**). Moreover, triplet lifetimes, τ_T, in the 630-1200 ns range were found for the Pt-Ar complexes (Table 2).

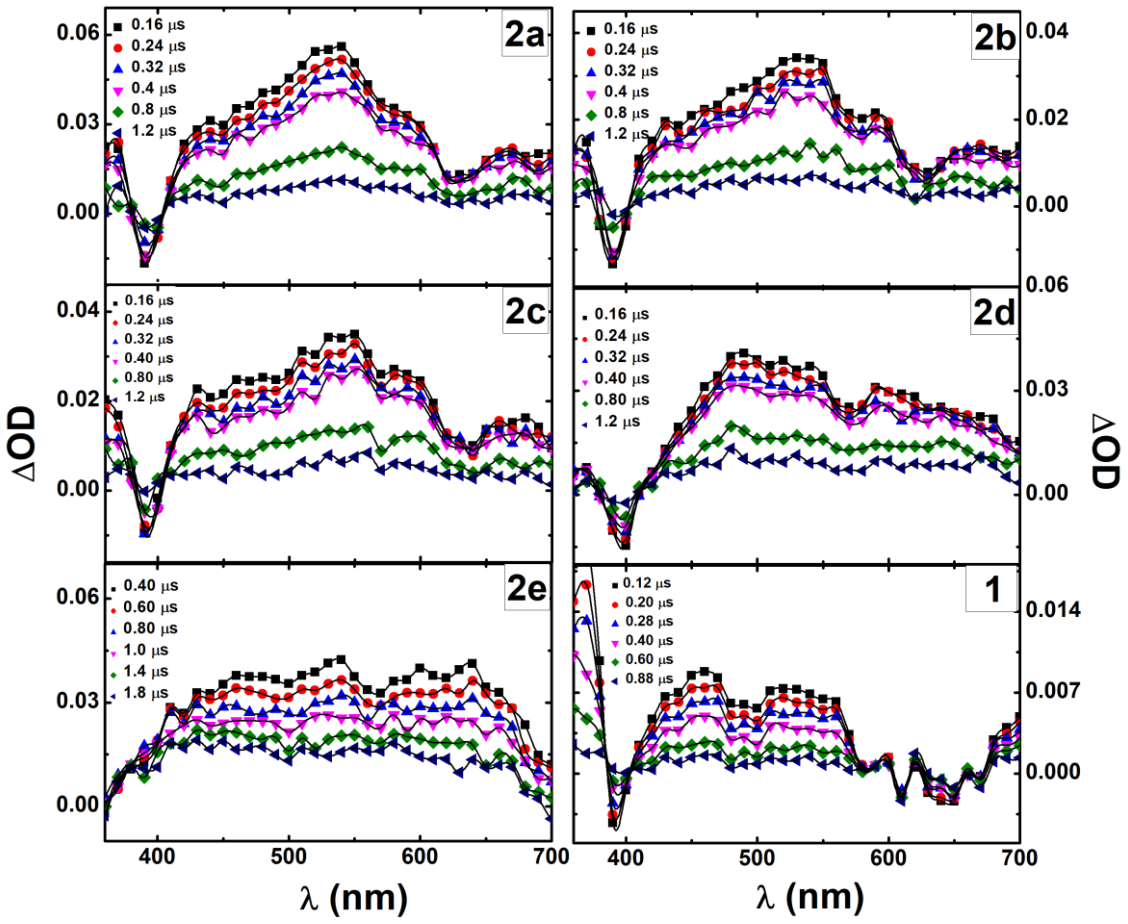

Figure 3. Room temperature time-resolved transient triplet-triplet absorption spectra for the Pt-Ar derivatives (**2a-e**) and Pt-Cl (**1**) collected by laser flash photolysis at 355 nm (ns-TA) in degassed acetonitrile solutions.

fs-transient absorption

Femtosecond (fs)-transient absorption (TA) provides additional information on the excited-state formation and deactivation processes occurring with the Pt-Ar complexes. The fs-TA data for Pt-Ar compounds and Pt-Cl spectra are dominated by strongly overlapped positive broad transient absorption bands in the 430-690 nm range, resulting

from the convolution of the singlet excited state absorption $ESA^{(S_1-S_n)}$ and the triplet excited state absorption, $ESA^{(T_1-T_n)}$. Although a strong overlap is observed between these characteristic bands the spectral resemblance of the bands observed at longer delay times in the fs-TA setup with the triplet-triplet absorption spectra obtained by ns-TA (see Figure 3), together with their long-lived nature (kinetics traces not decaying within the fs-TA probe time-window ~7.6 ns) these are assigned to the $T_1 \rightarrow T_n$ excited state absorption, following intersystem crossing.

The best-fit results and representative kinetic traces of the characteristic transient absorption data are presented in Table 3 and Figure 4. In general, the experimental kinetic traces are well fitted with the sum of three exponentials: (i) a first fast decay transient with values of ~ 200 fs; (ii) a second one with values ranging from 0.5 to 3.8 ps; (ii) and a long-lived transient associated to the triplet state decay that was fixed in the analysis to the triplet state lifetime obtained from the nanosecond laser flash photolysis, Table 3.

The fastest transient lifetimes are in good agreement with solvent relaxation time of acetonitrile (0.26 ps) and thus are assigned to the solvation dynamics.[24] While the 0.5-3.8 ps transient lifetimes are attributed to the decay of the singlet excited state which undergo rapid intersystem crossing ($\tau^{S_1 \sim\rightarrow T_1}$) to form the observed long lived triplet state. The observed negative amplitude values associated to the 0.5-3.8 ps transient lifetimes in the wavelength region where the $ESA^{(T_1-T_n)}$ occurs, together with the concentration profiles of the time constants and the distinct rise of the long-lived, 438 ns, time constant (see Figure 4 insets) supports the triplet state being formed at the expenses of the singlet excited state. The kinetic data obtained from the fs-TA experiments are in good agreement with the luminescence lifetimes obtained with nanosecond resolution from the time-correlated single photon counting (ns-TCSPC) technique, thus showing the decay from a triplet state with the $T_1 \rightarrow S_0$ transition becoming significantly allowed by the presence of the enhanced spin orbit coupling induced by Pt metal atom.

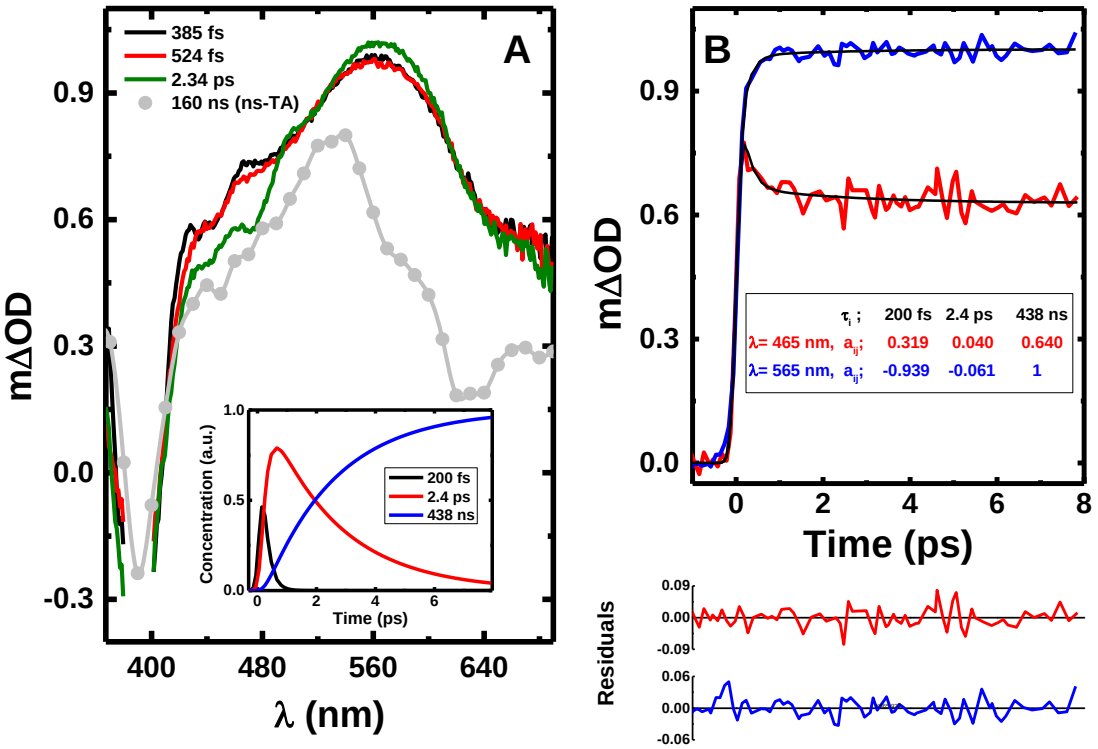

Figure 4. (A) Room temperature femtosecond time-resolved transient absorption data for **2a** collected in aerated acetonitrile solution with excitation at 390 nm, together with the normalized ns-ms transient absorption spectra collected at 160 ns after laser flash photolysis; as inset the concentration profiles of the time constants obtained from the analysis to the transient absorption data are presented; the fs-TA data in the spectral range 380-400 nm is not shown because it is disturbed by the scattered pump beam. **(B)** Representative kinetic traces with fits, lifetimes and pre-exponential values resulting from the analysis of the transient absorption data; for a better judgment of the quality of the fits the residuals are also shown.

Additionally, the intersystem crossing rate constants, $k'^{S_1 \sim\rightarrow T_1}_{ISC}$, can be calculated (assuming a unitary singlet oxygen sensitization efficiency, $S_D = \frac{f_T}{f_D} = 1$ and therefore $\phi_T \cong \phi_\Delta$) using the following equation 1,

$$k'^{S_1 \sim\rightarrow T_1}_{ISC} = \frac{\phi_T}{\tau^{S_1 \sim\rightarrow T_1}} \qquad \text{(equation 1)}$$

where the decay time and the quantum yield were obtained in aerated (presence of O_2) conditions.

The obtained $k'^{S_1 \sim\rightarrow T_1}_{ISC}$ values support the fast triplet state formation in the Pt-Ar (**2a-e**) complexes (Table 3).

Table 3. Intersystem crossing rate constants ($k'^{S_1 \sim \rightarrow T_1}_{ISC}$) obtained from the results of the global fit analysis to the fs-TA data of the Pt-Ar (**2a-e**) derivatives and Pt-Cl (**1**) in acetonitrile solution at 293K.

Compound	$\tau^{S_1 \sim \rightarrow T_1}$ (ps)	$k'^{S_1 \sim \rightarrow T_1}_{ISC}$ x10^{11} (s)
1	0.5	9.4
2a	2.4	0.8
2b	3.2	0.3
2c	2.9	1.0
2d	1.1	1.1
2e	3.8	0.4

Singlet oxygen production

The quantum yields of singlet oxygen sensitization for the Pt-Ar (**2a-e**) and the precursor Pt-Cl (**1**) were obtained by comparison of the near-infrared phosphorescence signal of $^1O_2$ at 1270 nm with that obtained for 1*H*-phenalen-1-one as reference (Table 2). Measurements were carried out in aerated acetonitrile solutions of the Pt-Ar complexes at room temperature.

It can be observed that the ϕ_Δ values obtained for the alkynyl ligands are 4 times higher than those of the corresponding platinum complexes (see comparison between Pt-Np (**2d**) and Np and Pt-Phen (**2e**) and Phen) (Table S2). The obtained ϕ_Δ values are more than one order of magnitude less than those measured for other platinum complexes recently reported in the literature[25–27] and in the same order of the produced by recently reported Pt(II) complexes displaying efficient biological activity.[1,10,28,29] Thus, in this case, the flexibility of the current [C^N^N'] ligand does not negatively affect (decrease) the resulting f_D values.

It seems that the presence of the platinum heavy atom increases the efficiency of the intersystem crossing (ISC) from $^1PS^*$ to $^3PS^*$ (PS = photosensitizer) and the long-lived

triplet state of PS ($^3PS^*$) is a crucial component for the generation of $^1O_2$[30] and for this, its importance is increasing in the last years and some examples have been found with very high $^1O_2$ photogeneration, being the Pt(II) species in the majority of the cases, attached to a macrocyclic structure (porphyrin or calixarene).[2,9,31–34]

From the values of the room temperature phosphorescence quantum yields obtained in the presence, f_{Ph}, and absence, f^0_{Ph}, of oxygen, the following Stern-Volmer type relation can be retrieved, assuming that the effect of oxygen in the singlet lifetime is negligible (which is the case, see fs-TA data and Table 3 for details):

$$\frac{f^0_{Ph}}{f_{Ph}} = 1 + \tau^o_{Ph} k_{ET} \qquad \text{(Equation 2)}$$

where τ^o_{Ph} is the phosphorescence decay time obtained in deaerated conditions and k_{ET}, the pseudo-unimolecular rate constant of energy transfer that leads to the formation of singlet oxygen (k_{ET} = k'[O_2] with $[O_2]_{acetonitrile}$ = 1.9×10^{-3} mol dm^{-3}).[35] The values of k_{ET} calculated with equation 2, are summarized in Table 2.

Additionally, the following relation can be achieved from the singlet oxygen quantum yield, f_D, and the ϕ_{Ph} values obtained in the presence of oxygen:

$$\frac{f_D}{f_{Ph}} = \frac{k_{ET}}{k_{Ph}} \qquad \text{(Equation 3)}$$

where k_{Ph} is the radiative rate constant for phosphorescence, easily obtained once k_{ET} is known. Finally, in aerated conditions the rate constant for intersystem crossing $T_1 \sim\!\!\rightarrow S_0$, $k_{ISC}^{T_1 \sim\!\!\rightarrow S_0}$, can be calculated using the following equation

$$k_{ISC}^{T_1 \sim\!\!\rightarrow S_0} = \frac{1}{\tau_{Ph}} - k_{Ph} - k_{ET} \qquad \text{(Equation 4)}$$

or through equation 5;

$$k_{ISC}^{T_1 \sim\!\!\rightarrow S_0} = \frac{1}{\tau^o_{Ph}} - k_{Ph} \qquad \text{(Equation 5)}$$

From Table 2 it can be seen that, in the absence of oxygen, the dominant excited state deactivation pathway is the radiationless internal conversion process (ϕ_{IC}) both for Pt-Cl (**1**) and Pt-Ar (**2a-e**).

Moreover, the phosphorescence quantum yields are very low even in the absence of oxygen. Interestingly, the pathway leading to singlet oxygen sensitization (k_{ET}) is highly competitive and always dominates with rate constants that are in some cases 4 times higher than internal conversion process, such is the case of **2a**. That is, despite the fact that the ancillary ligand does not produce noticeable effects in the range where the triplet emission occurs, it may introduce a very significant impact in the production of singlet oxygen.

The radiative rate constant for the triplet emission is also significantly affected by the aromatic ancillary ligand. Despite the values of k_{Ph} are always more than 10 times lower than the internal conversion, there is a significant increase (3 to 4 times) in k_{Ph} for compounds **2a**, **2b**, **2d** and **2e** when compared with compound **1**, that does not possess the ancillary ligand. Only in the case of the thiophene ligand (**2c**) this effect is not observed.

Theoretical studies

Theoretical calculations have been performed at DFT/B3LYP level to further understand the photophysical data. The minimum energy geometry conformation shows that, in all cases, the most stable expected conformation agrees with the X-ray crystal structures, displaying a perpendicular disposition between the aromatic rings of the chromophoric unit and the square-planar geometry around the cyclometallated unit (Figure S23) and validates the theoretical model.

As the spectra depends on the orientation of the aromatic group in the complex, calculations have been performed with the phenyl ring in **2a** in parallel, oblique or perpendicular disposition with respect to the metallacycle. As expected, the perpendicular disposition is the one that reproduces better the experimental data (Figure S24). Thus, this

conformation has been chosen for the calculations of all the spectra in acetonitrile (Figures S25-S35 and Tables S3-S4).

In all cases, the HOMO orbital is located at the Pt-alkynylchromophoric unit. The closest occupied orbitals HOMO-1 and HOMO-2 are located at the Pt-C≡C and aryl ring of the cyclometallated ligand while HOMO-3 is mainly located at the metal. The lowest unoccupied molecular orbital, LUMO, is centred on the π* orbital of the phenyl ring of the C^N ligand of the square-planar metallacycle. Thus, the lowest energy absorption transitions are assigned to ^{1}LLCT (C≡C → C^N)/^{1}MLCT transitions.

There are several high-energy transitions between 260-290 nm. The most intense (262 nm with f = 0.24 in the case of **2a**) corresponds mainly to a HOMO -> LUMO+4 transition. Both orbitals are mainly centered in the alkyne group, with a small contribution from the d-orbitals of the metal, and in the case of LUMO+4, also from the cyclometallated fragment; so they can be mainly regarded as π–π* IL transitions

The geometries of the complexes at the lowest singlet and triplet excited states were optimized and the corresponding transitions calculated in order to ascribe the observed emission transitions for both singlet and triplet emissions. Triplet emission is predicted with transitions between the LUMO+1/LUMO to HOMO/HOMO-1 orbitals (see Table 4). The predicted wavelengths for triplet emission is in agreement with the experimental data being another evidence for phosphorescence instead of fluorescence emission decays.

It can be observed that HOMO-1 and HOMO present some contribution of both metal and alkynyl chromophore while the LUMO is mainly located at the ligand from the metallacycle part of the molecule. For this reason, the observed transitions can be rationalized as a mixture of ^{3}IL and ^{3}MLCT transitions.

Table 4. Predicted singlet and triplet transitions for all complexes including the expected wavelength and the orbitals involved in the transition.

Complex	Singlet λ_{em} (nm) (f) / transition	Triplet λ_{em} (nm) / transition
1	457 (0.0174) LUMO → HOMO (88%)	629 LUMO → HOMO (81%)
2a	491 (0.0008) LUMO → HOMO (98%)	607 LUMO → HOMO-1 (77%) 522 LUMO → HOMO (97%)
2b	496 (0.0012) LUMO → HOMO (98%)	496 LUMO → HOMO-1 (75%) 429 LUMO → HOMO (96%)
2c	507 (0.0018) LUMO → HOMO (98%)	608 LUMO → HOMO-1 (76%) 548 LUMO → HOMO (97%)
2d	482 (0.2675) LUMO → HOMO (96%)	609 LUMO → HOMO-1 (78%) 536 LUMO+1 → HOMO (77%) 531 LUMO → HOMO (90%)
2e	514 (0.0226) LUMO → HOMO (96%)	608 LUMO → HOMO-1 (75%) 591 LUMO+1 → HOMO (88%) 550 LUMO → HOMO (96%)

Conclusions

The synthesis and a comprehensive photophysical characterization was undertaken for five novel cyclometallated platinum(II) compounds (Pt-Ar, **2a-e**). The absorption, emission and excitation spectra of Pt-Ar complexes are very similarly with the Pt-Cl cyclometallated compound (**1**) resulting to ^{1}LLCT /^{1}MLCT transitions for the absorption transitions and ^{3}IL and ^{3}MLCT transitions for the emission. DFT calculations have been an important tool to determine the orbitals involved in these transitions. Pt···Pt interactions are not involved in the photophysical properties of the compounds in agreement with the X-ray crystal structure resolved for three of the complexes. From different time-resolved (from fs to ns) spectroscopic techniques it is found that, at room temperature, the deactivation of the excited state leads to a fast formation of the T_1 state which subsequently deactivates (phosphorescence). The excited state is found to be

mainly located in the cyclometallated platinum chromophore unit. The formed triplet state is found to efficiently sensitize molecular oxygen with values ranging from 11% to 47%.

Experimental Section

General

All solvents used were of spectroscopic or equivalent grade. Acetonitrile was purchased from Sigma-Aldrich. Deoxygenation of the solutions was done by bubbling with a stream of argon or nitrogen for approximately 20 min in a device elsewhere described.[36] All measured solutions were freshly prepared (prior to the experiment).

All reagents were obtained from commercial sources and used as received. Ligand 4-$FC_6H_4CHN(CH_2)_2N(CH_3)_2$ (**L**) and compound $[PtCl\{(CH_3)_2N(CH_2)_2N{=}CH(4\text{-}FC_6H_3)\}]$ (**1**) were prepared as reported elsewhere. [11]

Physical Measurements.

Electrospray mass spectra were performed at the Unitat d'Espectrometria de Masses (Universitat de Barcelona) in a LC/MSD-TOF spectrometer using H_2O-CH_3CN 1:1 to introduce the sample. IR spectra were recorded in KBr dispersion on a FT-IR 520 Nicolet spectrophotometer. NMR spectra were recorded in $CDCl_3$ at the Unitat de RMN of the Universitat de Barcelona with a Mercury 400 spectrometer (^1H, 400 MHz; ^{19}F, 376.5 MHz). Chemical shifts are given in δ values (ppm) relative to TMS (^1H) or $CFCl_3$ (^{19}F) and coupling constants J are given in Hz. Numbering schemes for the compounds characterized are displayed in Scheme 1. Absorption spectra were obtained in a 5 mm or 10 mm quartz cuvette in acetonitrile on a Cary 5000 UV-vis-NIR or Shimadzu UV-2450 spectrophotometer. The emission spectra of the compounds in solution were obtained in fluorescence quartz cuvette of 5 mm or 10 mm path length, using a Horiba-Jobin-Vonn Fluorolog 3.22 or Fluoromax spectrometers. Phosphorescence spectra and decays were obtained with the D1934 unit of Fluoromax 3.22 spectrometer. All the fluorescence and phosphorescence spectra were corrected for the wavelength response of the system with the appropriate correction files obtained for the instrument. Microanalyses were performed at the Centres Científics i Tecnològics (Universitat de Barcelona).[11,37]

Emission Quantum Yield Determination and Laser Flash Photolysis Experiments.

All measured solutions were degassed using a cuvette specially designed and described elsewhere for 20-30 minutes with N_2 or Ar.[36] Emission quantum yields were determined with a Hamamatsu Quantaurus QY absolute photoluminescence quantum yield spectrometer model C11437 (integration sphere). Transient absorption spectra were measured using a flash photolysis setup composed of a LKS 60 ns laser photolysis spectrometer from Applied Photophysics, with a Brilliant Q-Switch Nd:YAG laser from Quantel, using the fourth harmonics (λ_{exc} = 355 nm, laser pulse half-width equal to 6 ns). The transient spectra were obtained by monitoring the optical density change at 5-10 nm intervals, averaging at least 10 decays at each wavelength.

Singlet Oxygen Yields.

Room-temperature singlet oxygen phosphorescence was detected at 1270 nm with an Horiba Jobin Ivon SPEX Fluorog 3.22 using the Hamamatsu R5509-42 photomultiplier previously reported. The use of a Schott RG1000 filter was essential to eliminate from the infrared signal all of the first harmonic contribution of sensitizer emission in the region below 850 m. The singlet oxygen formation quantum yield was then determined by direct measurement of the phosphorescence at 1270 nm following irradiation of the aerated solution of the samples in acetonitrile with excitation at 355 nm from a Nd:YAG laser with a setup elsewhere described. 1H-phenal-1-one in acetonitrile (ϕ_Δ = 0.98) was used as standard [38] applying eqn (6).

$$\Phi_\Delta{}^{cp} = \frac{slope^{cp}}{slope^{ref}} \cdot \frac{Abs_{cp}}{Abs_{ref}} \cdot \frac{n_{cp}^2}{n_{ref}^2} \cdot \Phi_\Delta{}^{ref} \qquad \text{(Equation 6)}$$

with ϕ_Δ^{ref} the singlet oxygen formation quantum yield of the reference compound. 1*H-phenal-1-one* in acetonitrile (ϕ_Δ = 0.98) was use as standard.

TCSPC.

Phosphorescence decays were obtained either in aerated or degassed acetonitrile solutions and were measured with two different home-built time-correlated single photon counting equipments (TCSPC). For the Pt-Ar (**2a-e**) and Pt-Cl (1) compounds a ns-TCSPC as elsewhere reported except that a nanoLED (excitation at 373 nm) IBH was used as the excitation source.[39] Deconvolution of the phosphorescence decay curves was performed

using the modulating function method, as implemented by G. Striker in the SAND program.[40]

fs-TA

The experimental setup for ultrafast spectroscopic and kinetic measurements was described elsewhere[41] and consists of a broadband (350–1600 nm) HELIOS pump–probe femtosecond transient absorption spectrometer from Ultrafast Systems, equipped with an amplified femtosecond Spectra-Physics Solstice-100F laser (800 nm central wavelength displaying a pulse width of 128 fs at 1 kHz repetition rate) coupled with a Spectra-Physics TOPAS Prime F optical parametric amplifier (195–22 000 nm) for pulse pump generation. Probe light in the UV range was generated by passing a small portion of the 800 nm light from the Solstice-100F laser through a computerized optical delay (with a time window up to 8 ns) and focusing in a vertical translating CaF_2 crystal to generate white-light continuum (350–750 nm). All measurements were obtained in a 2 mm quartz cuvette with absorptions lower than 0.3 at the pump excitation wavelength. The instrumental response function of the system was assumed to be equal to that of the pump–probe cross correlation determined from the measurement of the instantaneous stimulated Raman signal from the pure solvent (in a 2 mm cuvette). Typical values for the IRF of the system were found to be better than 250 fs. To avoid photodegradation the solutions were stirred during the experiments or in movement using a motorized translating sample holder. The spectral chirp of the data was corrected using Surface Xplorer PRO program from Ultrafast Systems. Global analysis of the data (using a sequential model) was performed after single value decomposition using Glotaran software.[42]

X-ray diffraction.

Single crystals suitable for X-ray diffraction analysis were grown for **2b**, **2c** and **2d** by slow diffusion of hexane in a dichloromethane solution of the compounds. The crystal data and experimental details for the data collections are given below. Single-crystal X-ray data for **2b**, **2c** and **2d** were collected at 170 K on a Bruker-Nonius KappaCCD diffractometer with an APEX-II detector with graphite-monochromatised Mo-Kα (λ = 0.71073 Å) radiation. Data collection was performed using the program COLLECT,[43] with data reduction performed using HKL DENZO and SCALEPACK,[44] with intensities absorption corrected using SADABS.[45] All structures were solved using ShelXT,[46] and

refined by full-matrix least squares on F^2 using SHELXL[47] in the OLEX2 program package.[48] Anisotropic displacement parameters were assigned to non-H atoms. Positional disorder in the structures was treated by gently restraining geometric and anisotropic displacement parameters. All hydrogen atoms were refined using riding models with U_{eq}(H) of 1.5U_{eq}(C). CCDC 1970145 - 1970147 contains the supplementary crystallographic data for this paper. These data can be obtained free of charge via http://www.ccdc.cam.ac.uk/conts/retrieving.html (or from the CCDC, 12 Union Road, Cambridge CB2 1EZ, UK; Fax: +44 1223 336033; E-mail: deposit@ccdc.cam.ac.uk). Crystallographic details are given in Table S1.

Theoretical Calculations.

DFT calculations have been performed using the Q-Chem[49] software implemented in Spartan'18,[50] with the B3LYP[51,52] functional and the following basis set: 6-31G*,[53,54] including polarization for non-nitrogen atoms, for C, H, N and Cl; and LANL2DZ[55] for Pt. Solvation effects have been included using the CPCM method.[56]

UV/Vis transitions have been calculated at the TD-DFT level using the same functional and basis set; this methodology have provided satisfactory results in our previous work.[57]

Preparation of the complexes

[Pt(C≡CPh){$(CH_3)_2N(CH_2)_2N$=CH(4-FC_6H_3)}] (**2a**) was obtained from the reaction of 0.103 g (0.243 mmols) of [PtCl{$(CH_3)_2N(CH_2)_2N$=CH(4-FC_6H_3)}] (**1**), 0.025 g (0.249 mmols) of phenylacetylene, 0.010 g (0.053 mmols) of CuI and 0.061 g (0.744 mmols) of sodium acetate in CH_2Cl_2/Methanol (10:1). The mixture was stirred at room temperature under nitrogen and protected from light for 48 hours. The solvent was removed under vacuum and the residue was treated with hexane. The orange solid was filtered and dried under vacuum. Yield: 0.091 g (76%). **^{1}H NMR** ($CDCl_3$, 400 MHz): δ 8.32 [s, 1H, ^{3}J(Pt-H) = 81.2, H^d]; 7.55 [dd, 1H, ^{3}J(F-H) = 9.6, ^{4}J(H-H) = 2.3, ^{3}J(Pt-H) = 70.2, H^a], 7.48 [d, 2H, ^{3}J(H-H) = 7.1, H^{Ph}], 7.22-7.24 [m, 3H, $H^{c,Ph}$], 7.15 [t, 1H, ^{3}J(H-H) = 7.4, H^{Ph}], 6.66 [td, 1H, ^{3}J(F-H) = ^{3}J(H-H) = 8.8, ^{4}J(H-H) = 2.6, H^b], 4.01 [t, ^{3}J(H-H) = 11.7, 2H, H^e], 3.15 [t, 2H, ^{3}J(H-H) = 6.0 Hz, H^f], 3.06 [s, 6H, ^{3}J(Pt-H) = 20.2, H^g]. **^{19}F NMR** ($CDCl_3$, 376.5 MHz): δ -108.44 [s, 1F]. **MS-ESI$^+$**: *m/z* 490.12 $[M + H]^+$. **IR**: υ 2097.10 (C≡C). Anal. Found (calcd for $C_{19}H_{19}FN_2Pt\cdot\cdot0.5\ CH_2Cl_2$): C 44.86 (44.03); H 3.52 (3.79); N 5.24 (5.27).

[Pt(C≡CPh-F){$(CH_3)_2N(CH_2)_2N$=CH(4-FC_6H_3)}] (**2b**) was prepared as an orange solid by following the same method from 0.102 g (0.241 mmols) of [PtCl{$(CH_3)_2N(CH_2)_2N$=CH(4-FC_6H_3)}] (**1**), 0.030 g (0.249 mmols) of 1-ethynyl-4-fluorobenzene, 0.010 g (0.053 mmols) of CuI and 0.063 g (0.768 mmols) of sodium acetate. Yield: 0.070 g (57%). **^{1}H NMR** ($CDCl_3$, 400 MHz): δ 8.34 [s, 1H, ^{3}J(Pt-H) = 81.3, H^d], 7.53 [dd, 1H, ^{3}J(F-H) = 9.4, ^{4}J(H-H) = 2.7, ^{3}J(Pt-H) = 71.1, H^a], 7.43 [dd, J = 8.9, 5.5 Hz, 2H, H^{Ph-F}], 7.23 [m, 1H, H^c], 6.93 [t, 2H, ^{3}J(F-H) = ^{3}J(H-H) = 8.9 , H^{Ph-F}], 6.67 [td, 1H, ^{3}J(F-H) = ^{3}J(H-H) = 8.6, ^{4}J(H-H) = 2.6, H^b], 4.03 [t, 2H, ^{3}J(H-H) = 5.9 ,H^e], 3.15 [t, 2H, ^{3}J(H-H) = 6.0, H^f], 3.04 [s, 6H, ^{3}J(Pt-H) = 20.2, H^g]. **^{19}F NMR** ($CDCl_3$, 376.5 MHz): δ -103.98 [s, 1F]; -115.55 [s, 1F, F^a]. **MS-ESI$^+$**: *m/z* 508.12 $[M + H]^+$. **IR**: υ 2100.26 (C≡C). Anal. Found (calcd for $C_{19}H_{18}F_2N_2Pt{\cdot}0.5\ CH_2Cl_2$): C 42.59 (42.59); H 3.29 (3.48); N 5.12 (5.09).

[Pt(C≡CThio){$(CH_3)_2N(CH_2)_2N$=CH(4-FC_6H_3)}] (**2c**) was prepared as an orange solid by following the same method from 0.099 g (0.243 mmols) of [PtCl{$(CH_3)_2N(CH_2)_2N$=CH(4-FC_6H_3)}] (**1**), 0.027 g (0.249 mmols) of 3-ethynyltiophene, 0.010 g (0.053 mmols) of CuI and 0.060 g (0.731 mmols) of sodium acetate. Yield: 0.086 g (74%). **^{1}H NMR** ($CDCl_3$, 400 MHz): δ 8.35 [s, 1H, ^{3}J(Pt-H) = 80.9, H^d], 7.56 [dd, 1H, ^{3}J(F-H) = 9.6, ^{4}J(H-H) = 2.7, ^{3}J(Pt-H) = 70.7, H^a], 7.24 [m, 2H, $H^{c,Tioph}$], 7.19 [dd, 1H, ^{3}J(H-H) = 4.9, ^{3}J(H-H) = 3.0, H^{Tioph}], 7.14 [dd, 1H, ^{3}J(H-H) = 4.9, ^{3}J(H-H) = 1.1, H^{Tioph}], 6.66 [td, 1H, ^{3}J(F-H) = ^{3}J(H-H) = 8.6, ^{4}J(H-H) = 2.5, H^b], 4.03 [t, 2H, ^{3}J(H-H) = 6.4, H^e], 3.14 [t, 2H, ^{3}J(H-H) = 6.0, H^f], 3.04 [s, 6H, ^{3}J(Pt-H) = 20.5, H^g]. **^{19}F NMR** ($CDCl_3$, 376.5 MHz): δ -104.17 [s, 1F]. **MS-ESI$^+$**: *m/z* 496.08 $[M + H]^+$. **IR**: υ 2104.33 (C≡C). Anal. Found (calcd. for $C_{17}H_{17}FN_2PtS{\cdot}0.5\ CH_2Cl_2$): C 39.07 (39.52); H 3.34 (3.37); N 5.31 (5.21); S 5.77 (5.96).

[Pt(C≡CNaph){$(CH_3)_2N(CH_2)_2N$=CH(4-FC_6H_3)}] (**2d**) was prepared as an orange solid by following the same method from 0.051 g (0.120 mmols) of [PtCl{$(CH_3)_2N(CH_2)_2N$=CH(4-FC_6H_3)}] (**1**), 0.019 g (0.125 mmols) of 2-ethynylnaphthalene, 0.005 g (0.026 mmols) of CuI and 0.029 g (0.359 mmols) of sodium acetate. Yield: 0.050 g (77%). **^{1}H NMR** ($CDCl_3$, 400 MHz): δ 8.36 [s, 1H, ^{3}J(Pt-H) = 79.5, H^d], 7.92 [s, 1H, H^{Naph}]; 7.74 [t, 2H, ^{3}J(H-H) = 6.7, H^{Naph}]; 7.70 [d, 1H, ^{3}J(H-H) = 8.4, H^{Naph}]; 7.64 [d, 1H, ^{3}J(F-H) = 10.4, H^a]; 7.57 [d, 1H, ^{3}J(H-H) = 8.4, H^{Naph}]; 7.39 [m, 2H, H^{Naph}]; 7.26 [m, 1H, H^c]; 6.68 [t, 1H, ^{3}J(F-H) = ^{3}J(H-H) = 8.8, H^b], 4.04 [t, 2H, ^{3}J(H-H) = 6.2, H^e], 3.17 [t, 2H, ^{3}J(H-H) = 5.4, H^f], 3.10 [s, 6H, ^{3}J(Pt-H) = 19.6, H^g]. **^{19}F NMR**

($CDCl_3$, 376.5 MHz): δ -104.16 [s, 1F]. **MS-ESI$^+$**: *m/z* 539.14 $[M + H]^+$. **IR**: υ 2099.88 (C≡C).

[Pt(C≡CPhen){$(CH_3)_2N(CH_2)_2N$=CH(4-FC_6H_3)}] (**2e**) was prepared as an orange solid by following the same method from 0.052 g (0.123 mmols) of [PtCl{$(CH_3)_2N(CH_2)_2N$=CH(4-FC_6H_3)}] (**1**), 0.025 g (0.125 mmols) of 9-ethynylphenanthrene, 0.005 g (0.026 mmols) of CuI and 0.031 g (0.378 mmols) of sodium acetate. Yield: 0.061 g (84%). **^{1}H NMR** ($CDCl_3$, 400 MHz): δ 8.81 [m, 1H, H^{Phen}]; 8.65 [m, 1H, H^{Phen}]; 8.61 [d, ^{3}J(H-H) = 7.8, 1H, H^{Phen}]; 8.30 [s, 1H, ^{3}J(Pt-H) = 81.9, H^d], 7.96 [s, 1H, H^{Phen}]; 7.79 [d, ^{3}J(H-H) = 7.3, 1H, H^a]; 7.68 [dd, 1H, ^{3}J(H-H) = 9.6, ^{4}J(H-H) = 2.3, H^{Phen}], 7.63 [m, 2H, H^{Phen}]; 7.55 [m, 2H, H^{Phen}]; 7.26 [m, 1H, H^c], 6.68 [td, 1H, ^{3}J(F-H) = ^{3}J(H-H) = 8.5, ^{4}J(H-H) = 2.6, H^b], 4.53 [t, 2H, ^{3}J(H-H) = 6.2, H^e], 3.18 [t, 2H, ^{3}J(H-H) = 5.9, H^f], 3.12 [s, 6H, ^{3}J(Pt-H) = 19.3, H^g]. **^{19}F NMR** ($CDCl_3$, 376.5 MHz): δ -103.86 [s, 1F]. **MS-ESI$^+$**: *m/z* 590.16 $[M + H]^+$. **IR**: υ 2078.10 (C≡C).

Supporting Information

^{1}H, ^{19}F NMR and ESI-MS(+) spectra of the compounds. Absorption, emission and excitation data. X-ray crystal data (unit cell and packing, crystal data and refinement) of **2b**, **2c** and **2d**. Representation of the minimum energy geometry conformation, orbitals and coordenates involved in the transitions and calculated UV-visible spectra of the cyclometallated complexes.

Acknowledgements

The authors are grateful to Spanish Ministerio de Ciencia, Innovación y Universidades (AEI/FEDER, UE Project CTQ2016-76120-P and CTQ2015-65040-P). FCT/MCTES is acknowledged for financial support through the Associate Laboratory for Green Chemistry, LAQV-REQUIMTE (UID/QUI/50006/2013), the Coimbra Chemistry Centre (UID/QUI/00313/2019) and through Project PTDC/QUI-QFI/32007/2017 and Project "Hylight" (no. 031625) 02/SAICT/2017. We acknowledge funding by Fundo Europeu de Desenvolvimento Regional (FEDER) through Programa Operacional Factores de Competitividade (COMPETE) and project ROTEIRO/0152/2013. The research leading to these results has received funding from Laserlab-Europe (grant agreement no. 284464, EC's Seventh Framework Programme).

References

(1) Goswami, S.; Winkel, R. W.; Schanze, K. S. Photophysics and Nonlinear Absorption of Gold(I) and Platinum(II) Donor–Acceptor–Donor Chromophores. *Inorg. Chem.* **2015**, *54* (20), 10007–10014. https://doi.org/10.1021/acs.inorgchem.5b01767.

(2) Jiang, X.; Zhu, N.; Zhao, D.; Ma, Y. New Cyclometalated Transition-Metal Based Photosensitizers for Singlet Oxygen Generation and Photodynamic Therapy. *Sci. China Chem.* **2016**, *59* (1), 40–52. https://doi.org/10.1007/s11426-015-5519-2.

(3) Rogers, J. E.; Slagle, J. E.; Krein, D. M.; Burke, A. R.; Hall, B. C.; Fratini, A.; McLean, D. G.; Fleitz, P. A.; Cooper, T. M.; Drobizhev, M.; et al. Platinum Acetylide Two-Photon Chromophores. *Inorg. Chem.* **2007**, *46* (16), 6483–6494. https://doi.org/10.1021/ic700549n.

(4) Mei, J.; Ogawa, K.; Kim, Y.-G.; Heston, N. C.; Arenas, D. J.; Nasrollahi, Z.; McCarley, T. D.; Tanner, D. B.; Reynolds, J. R.; Schanze, K. S. Low-Band-Gap Platinum Acetylide Polymers as Active Materials for Organic Solar Cells. *ACS Appl. Mater. Interfaces* **2009**, *1* (1), 150–161. https://doi.org/10.1021/am800104k.

(5) Giménez, N.; Lalinde, E.; Lara, R.; Moreno, M. T. Design of Luminescent, Heteroleptic, Cyclometalated Pt II and Pt IV Complexes: Photophysics and Effects of the Cyclometalated Ligands. *Chem. – A Eur. J.* **2019**, *25* (21), 5514–5526. https://doi.org/10.1002/chem.201806240.

(6) Millán, G.; Giménez, N.; Lara, R.; Berenguer, J. R.; Moreno, M. T.; Lalinde, E.; Alfaro-Arnedo, E.; López, I. P.; Pineiro-Hermida, S.; Pichel, J. G. Luminescent Cycloplatinated Complexes with Biologically Relevant Phosphine Ligands: Optical and Cytotoxic Properties. *Inorg. Chem.* **2019**, *58* (2), 1657–1673. https://doi.org/10.1021/acs.inorgchem.8b03211.

(7) Herberger, J.; Winter, R. F. Platinum Emitters with Dye-Based r -Aryl Ligands. *Coord. Chem. Rev.* **2019**, *400*, 213048. https://doi.org/10.1016/j.ccr.2019.213048.

(8) Bandeira, S.; Gonzalez-Garcia, J.; Pensa, E.; Albrecht, T.; Vilar, R. A Redox-Activated G-Quadruplex DNA Binder Based on a Platinum(IV)–Salphen Complex. *Angew. Chemie - Int. Ed.* **2018**, *57* (1), 310–313. https://doi.org/10.1002/anie.201709968.

(9) McKenzie, L. K.; Bryant, H. E.; Weinstein, J. A. Transition Metal Complexes as Photosensitisers in One- and Two-Photon Photodynamic Therapy. *Coord. Chem. Rev.* **2019**, *379*, 2–29. https://doi.org/10.1016/j.ccr.2018.03.020.

(10) Geist, F.; Jackel, A.; Irmler, P.; Linseis, M.; Malzkuhn, S.; Kuss-Petermann, M.; Wenger, O. S.; Winter, R. F. Directing Energy Transfer in Panchromatic Platinum Complexes for Dual Vis-Near-IR or Dual Visible Emission from σ-Bonded BODIPY Dyes. *Inorg. Chem.* **2017**, *56* (2), 914–930. https://doi.org/10.1021/acs.inorgchem.6b02549.

(11) Gandioso, A.; Valle-Sistac, J.; Rodríguez, L.; Crespo, M.; Font-Bardía, M. Platinum(II) Compounds Containing Cyclometalated Tridentate Ligands: Synthesis, Luminescence Studies, and a Selective Fluoro for Methoxy Substitution. *Organometallics* **2014**, *33* (2), 561–570. https://doi.org/10.1021/om401111t.

(12) Lázaro, A.; Serra, O.; Rodríguez, L.; Crespo, M.; Font-Bardia, M. Luminescence Studies of New [C,N,N′] Cyclometallated Platinum(Ii) and Platinum(Iv) Compounds. *New J. Chem.* **2019**, *43* (3), 1247–1256. https://doi.org/10.1039/c8nj05492d.

(13) Sierra, H.; Cordova, M.; Chen, C.-S. J.; Rajadhyaksha, M. Confocal Imaging–Guided Laser Ablation of Basal Cell Carcinomas: An Ex Vivo Study. *J. Invest. Dermatol.* **2015**, *135* (2), 612–615. https://doi.org/10.1038/jid.2014.371.

(14) Shavaleev, N. M.; Adams, H.; Best, J.; Edge, R.; Navaratnam, S.; Weinstein, J. A. Deep-Red Luminescence and Efficient Singlet Oxygen Generation by Cyclometalated Platinum(II) Complexes with 8-Hydroxyquinolines and Quinoline-8-Thiol. *Inorg. Chem.* **2006**, *45* (23), 9410–9415. https://doi.org/10.1021/ic061283k.

(15) Haque, A.; Xu, L.; Al-Balushi, R. A.; Al-Suti, M. K.; Ilmi, R.; Guo, Z.; Khan, M.

S.; Wong, W. Y.; Raithby, P. R. Cyclometallated Tridentate Platinum(Ii) Arylacetylide Complexes: Old Wine in New Bottles. *Chem. Soc. Rev.* **2019**, *48* (23), 5547–5563. https://doi.org/10.1039/c8cs00620b.

(16) Zhang, W.; Luo, Y.; Xu, Y.; Tian, L.; Li, M.; He, R.; Shen, W. The Electronic Structures and Photophysical Properties of Platinum Complexes with C^N^N Ligands: The Influence of the Carborane Substituent. *Dalt. Trans.* **2015**, *44* (41), 18130–18137. https://doi.org/10.1039/C5DT02110C.

(17) Lu, W.; Mi, B.-X.; Chan, M. C. W.; Hui, Z.; Che, C.-M.; Zhu, N.; Lee, S.-T. Light-Emitting Tridentate Cyclometalated Platinum(II) Complexes Containing σ-Alkynyl Auxiliaries: Tuning of Photo- and Electrophosphorescence. *J. Am. Chem. Soc.* **2004**, *126* (15), 4958–4971. https://doi.org/10.1021/ja0317776.

(18) Savel, P.; Latouche, C.; Roisnel, T.; Akdas-Kilig, H.; Boucekkine, A.; Fillaut, J.-L. Cyclometalated Platinum(Ii) with Ethynyl-Linked Azobenzene Ligands: An Original Switching Mode. *Dalt. Trans.* **2013**, *42* (48), 16773. https://doi.org/10.1039/c3dt51925b.

(19) Lanoë, P.-H.; Bozec, H. Le; Gareth Williams, J. A.; Fillaut, J.-L.; Guerchais, V. Cyclometallated Platinum(Ii) Complexes Containing Pyridyl-Acetylide Ligands: The Selective Influence of Lead Binding on Luminescence. *Dalton Trans.* **2010**, *39* (3), 707–710. https://doi.org/10.1039/B914957K.

(20) Sonogashira, K.; Fujikura, Y.; Yatake, T.; Toyoshima, N.; Takahashi, S.; Hagihara, N. Syntheses and Properties of Cis- and Trans-Dialkynyl Complexes of Platinum(II). *J. Organomet. Chem.* **1978**, *145* (1), 101–108. https://doi.org/10.1016/S0022-328X(00)84078-4.

(21) Puttock, E. V.; Walden, M. T.; Williams, J. A. G. The Luminescence Properties of Multinuclear Platinum Complexes. *Coord. Chem. Rev.* **2018**, *367*, 127–162. https://doi.org/10.1016/j.ccr.2018.04.003.

(22) Li, K.; Wan, Q.; Yang, C.; Chang, X. Y.; Low, K. H.; Che, C. M. Air-Stable Blue Phosphorescent Tetradentate Platinum(II) Complexes as Strong Photo-Reductant. *Angew. Chemie - Int. Ed.* **2018**, *57* (43), 14129–14133. https://doi.org/10.1002/anie.201808642.

(23) Viola, E.; Donzello, M. P.; Ercolani, C.; Rizzoli, C.; Lever, A. B. P. Synthesis and Structure of Rare Zwitterionic Complexes Involving the Presence of N(Py)MCl3− Moieties (M = Pt(II), Pd(II)). *Inorganica Chim. Acta* **2018**, *480*, 101–107. https://doi.org/10.1016/j.ica.2018.04.031.

(24) Horng, M. L.; Gardecki, J. A.; Papazyan, A.; Maroncelli, M. Subpicosecond Measurements of Polar Solvation Dynamics: Coumarin 153 Revisited. *J. Phys. Chem.* **1995**, *99* (48), 17311–17337. https://doi.org/10.1021/j100048a004.

(25) Toubia, I.; Nguyen, C.; Diring, S.; Ali, L. M. A.; Larue, L.; Aoun, R.; Frochot, C.; Gary-Bobo, M.; Kobeissi, M.; Odobel, F. Synthesis and Anticancer Activity of Gold Porphyrin Linked to Malonate Diamine Platinum Complexes. *Inorg. Chem.* **2019**, *58* (18), 12395–12406. https://doi.org/10.1021/acs.inorgchem.9b01981.

(26) Yao, S.; Chen, L.; Jia, F.; Sun, X.; Su, H.; Liu, H.; Yang, L.; Wang, Z.; Liu, F.; Wang, K. Platinated Porphyrin Tailed with Folic Acid Conjugate for Cell-Targeted Photodynamic Activity. *J. Lumin.* **2019**, *214* (June), 116552. https://doi.org/10.1016/j.jlumin.2019.116552.

(27) Yang, M.; Deng, J.; Guo, D.; Zhang, J.; Yang, L.; Wu, F. A Folate-Conjugated Platinum Porphyrin Complex as a New Cancer-Targeting Photosensitizer for Photodynamic Therapy. *Org. Biomol. Chem.* **2019**, *17* (21), 5367–5374. https://doi.org/10.1039/c9ob00698b.

(28) Shi, H.; Clarkson, G. J.; Sadler, P. J. Dual Action Photosensitive Platinum(II) Anticancer Prodrugs with Photoreleasable Azide Ligands. *Inorganica Chim. Acta* **2019**, *489* (February), 230–235. https://doi.org/10.1016/j.ica.2019.02.016.

(29) Xue, X.; Zhu, C.; Chen, H.; Bai, Y.; Shi, X.; Jiao, Y.; Chen, Z.; Miao, Y.; He, W.; Guo, Z. A New Approach to Sensitize Antitumor Monofunctional Platinum(II) Complexes via Short Time Photo-Irradiation. *Inorg. Chem.* **2017**, *56* (7), 3754–3762. https://doi.org/10.1021/acs.inorgchem.6b02148.

(30) Kim, S.; Ohulchanskyy, T. Y.; Bharali, D.; Chen, Y.; Pandey, R. K.; Prasad, P. N. Organically Modified Silica Nanoparticles with Intraparticle Heavy-Atom Effect on the Encapsulated Photosensitizer for Enhanced Efficacy of

Photodynamic Therapy. *J. Phys. Chem. C* **2009**, *113* (29), 12641–12644. https://doi.org/10.1021/jp900573s.

(31) Lai, S. W.; Liu, Y.; Zhang, D.; Wang, B.; Lok, C. N.; Che, C. M.; Selke, M. Efficient Singlet Oxygen Generation by Luminescent 2-(2′-Thienyl) Pyridyl Cyclometalated Platinum(II) Complexes and Their Calixarene Derivatives. *Photochem. Photobiol.* **2010**, *86* (6), 1414–1420. https://doi.org/10.1111/j.1751-1097.2010.00809.x.

(32) Jana, A.; McKenzie, L.; Wragg, A. B.; Ishida, M.; Hill, J. P.; Weinstein, J. A.; Baggaley, E.; Ward, M. D. Porphyrin/Platinum(II) C^N^N Acetylide Complexes: Synthesis, Photophysical Properties, and Singlet Oxygen Generation. *Chem. - A Eur. J.* **2016**, *22* (12), 4164–4174. https://doi.org/10.1002/chem.201504509.

(33) Pushpanandan, P.; Maurya, Y. K.; Omagari, T.; Hirosawa, R.; Ishida, M.; Mori, S.; Yasutake, Y.; Fukatsu, S.; Mack, J.; Nyokong, T.; et al. Singly and Doubly N-Confused Calix[4]Phyrin Organoplatinum(II) Complexes as Near-IR Triplet Sensitizers. *Inorg. Chem.* **2017**, *56* (20), 12572–12580. https://doi.org/10.1021/acs.inorgchem.7b02047.

(34) Hu, X.; Ogawa, K.; Kiwada, T.; Odani, A. Water-Soluble Metalloporphyrinates with Excellent Photo-Induced Anticancer Activity Resulting from High Tumor Accumulation. *J. Inorg. Biochem.* **2017**, *170*, 1–7. https://doi.org/10.1016/j.jinorgbio.2017.02.001.

(35) Ware, W. R.; Cunningham, P. T. Fluorescence Lifetime and Fluorescence Enhancement of Perylene Vapor. *J. Chem. Phys.* **1966**, *44* (11), 4364–4365. https://doi.org/10.1063/1.1726640.

(36) Seixas de Melo, J. S. The Influence of Oxygen on the Lifetime of Luminescent Probes. A Simple Device for Degassing Solutions for Fluorescence Measurements . *Chem . Educ.* **2005**, *10* (05), 29–35.

(37) The analyses of fluorinated compounds present significant difficulty; see: Fadeeva, V. P.; Tikhova, V. D.; Nikulicheva, O. N. *J. Anal. Chem*. **2008**, *63*, 1094−1106. The analysis obtained for 2a-c are the best obtained data and have been included in the text. NMR and excitation spectra can support the purity of

all compounds.

(38) Kristiansen, M.; Scurlock, R. D.; Iu, K. K.; Ogilby, P. R. Charge-Transfer State and Singlet Oxygen (1.DELTA.g O2) Production in Photoexcited Organic Molecule-Molecular Oxygen Complexes. *J. Phys. Chem.* **1991**, *95* (13), 5190–5197. https://doi.org/10.1021/j100166a051.

(39) Seixas de Melo, J.; Fernandes, P. . Spectroscopy and Photophysics of 4- and 7-Hydroxycoumarins and Their Thione Analogs. *J. Mol. Struct.* **2001**, *565–566*, 69–78. https://doi.org/10.1016/S0022-2860(01)00458-6.

(40) Striker, G.; Subramaniam, V.; Seidel, C. A. M.; Volkmer, A. Photochromicity and Fluorescence Lifetimes of Green Fluorescent Protein. *J. Phys. Chem. B* **1999**, *103* (40), 8612–8617. https://doi.org/10.1021/jp991425e.

(41) Pina, J.; Seixas de Melo, J. S.; Eckert, A.; Scherf, U. Unusual Photophysical Properties of Conjugated, Alternating Indigo–Fluorene Copolymers. *J. Mater. Chem. A* **2015**, *3* (12), 6373–6382. https://doi.org/10.1039/C4TA06272H.

(42) Snellenburg, J. J.; Laptenok, S. P.; Seger, R.; Mullen, K. M.; Stokkum, I. H. M. van. Glotaran : A Java -Based Graphical User Interface for the R Package TIMP. *J. Stat. Softw.* **2012**, *49* (3), 1–22. https://doi.org/10.18637/jss.v049.i03.

(43) R. W. W. Hooft, COLLECT **1998**, Nonius BV, Delft, The Netherlands.

(44) Otwinowski, Z., Minor, W., Methods in Enzymology, Macromolecular Crystallography, Part A **1997**, 276, 307-326. Edited by C. W. Carter Jr & R. M. Sweet, New York: Academic Press.

(45) Sheldrick, G. M., SADABS Version 2008/2 **1996**, University of Göttingen, Germany.

(46) Sheldrick, G. M. SHELXT - Integrated space-group and crystal-structure determination *Acta Cryst.* **2015**, *A71*, 3-8.

(47) Sheldrick, G. M. Crystal structure refinement with SHELXL. *Acta Cryst.*, **2015**, *C71*, 3-8.

(48) Dolomanov, O. V., Bourhis, L. J., Gildea, R. J., Howard, J. A. K.; Puschmann,

H., OLEX2: a complete structure solution, refinement and analysis program. *J. Appl. Cryst.* **2009**, *42*, 339-341.

(49) Shao, Y.; Gan, Z.; Epifanovsky, E.; Gilbert, A. T. B.; Wormit, M.; Kussmann, J.; Lange, A. W.; Behn, A.; Deng, J.; Feng, X.; et al. Advances in Molecular Quantum Chemistry Contained in the Q-Chem 4 Program Package. *Mol. Phys.* **2015**, *113* (2), 184–215. https://doi.org/10.1080/00268976.2014.952696.

(50) Spartan'18 v. 1.4.0. Wavefunction, Inc.: Irvine, CA. **2019**.

(51) Becke, A. D. Density-Functional Thermochemistry. III. The Role of Exact Exchange. *J. Chem. Phys.* **1993**, *98* (7), 5648–5652. https://doi.org/10.1063/1.464913.

(52) Lee, C.; Yang, W.; Parr, R. G. Development of the Colle-Salvetti Correlation-Energy Formula into a Functional of the Electron Density. *Phys. Rev. B* **1988**, *37* (2), 785–789. https://doi.org/10.1103/PhysRevB.37.785.

(53) Hariharan, P. C.; Pople, J. A. The Influence of Polarization Functions on Molecular Orbital Hydrogenation Energies. *Theor. Chim. Acta* **1973**, *28* (3), 213–222. https://doi.org/10.1007/BF00533485.

(54) Francl, M. M.; Pietro, W. J.; Hehre, W. J.; Binkley, J. S.; Gordon, M. S.; DeFrees, D. J.; Pople, J. A. Self-consistent Molecular Orbital Methods. XXIII. A Polarization-type Basis Set for Second-row Elements. *J. Chem. Phys.* **1982**, *77* (7), 3654–3665. https://doi.org/10.1063/1.444267.

(55) Hay, P. J.; Wadt, W. R. Ab Initio Effective Core Potentials for Molecular Calculations. Potentials for K to Au Including the Outermost Core Orbitals. *J. Chem. Phys.* **1985**, *82* (1), 299–310. https://doi.org/10.1063/1.448975.

(56) Cossi, M.; Rega, N.; Scalmani, G.; Barone, V. Energies, Structures, and Electronic Properties of Molecules in Solution with the C-PCM Solvation Model. *J. Comput. Chem.* **2003**, *24* (6), 669–681. https://doi.org/10.1002/jcc.10189.

(57) Bartocci, S.; Sabaté, F.; Bosque, R.; Keymeulen, F.; Bartik, K.; Rodríguez, L.; Dalla Cort, A. Colorimetric and Fluorescence "Turn-on" Recognition of Fluoride by a Maleonitrile-Based Uranyl Salen-Complex. *Dye. Pigment.* **2016**, *135*, 94–

101. https://doi.org/10.1016/j.dyepig.2016.06.006.

Graphical Abstract

Platinum cyclometallated compounds containing alkynyl chromophores have been synthesized and fully characterized. The X-ray crystal structures of three of the complexes do not show Pt···Pt contacts. Their photophysical properties have been studied in detail showing room temperature phosphorescence (RTP) and efficient $^1O_2$ production.